J. Fluid Mech. (1991), *vol.* 224, *pp.* 177–196
Printed in Great Britain

Vortex ring bubbles

By T. S. LUNDGREN[1] AND N. N. MANSOUR[2]

[1] Department of Aerospace Engineering and Mechanics, University of Minnesota, Minneapolis, MN 55455, USA

[2] NASA Ames Research Center, Moffett Field, CA 94035, USA

(Received 27 February 1990)

Toroidal bubbles with circulation are studied numerically and by means of a physically motivated model equation. Two series of computations are performed by a boundary-integral method. One set shows the starting motion of an initially spherical bubble as a gravitationally driven liquid jet penetrates through the bubble from below causing a toroidal geometry to develop. The jet becomes broader as surface tension increases and fails to penetrate if surface tension is too large. The dimensionless circulation that develops is not very dependent on the surface tension. The second series of computations starts from a toroidal geometry, with circulation determined from the earlier series, and follows the motion of the rising and spreading vortex ring. Some modifications to the boundary-integral formulation were devised to handle the multiply connected geometry. The computations uncovered some unexpected rapid oscillations of the ring radius. These oscillations and the spreading of the ring are explained by the model equation which provides a more general description of vortex ring bubbles than previously available.

1. Introduction

Vortex ring bubbles are fairly easy to create. There is a photograph in the *National Geographic Magazine* (Earle & Giddings 1976) which shows a diver (Giddings) twenty feet below the surface, exhaling a series of toroidal bubbles. These are air-core vortex rings, with approximately constant core volumes perhaps as large as half a litre, which expand to be rings of the order of two feet in diameter as they rise towards the surface. J. G. Brasseur (private communication, 1989) observed a dolphin at Sea World, San Francisco to blow a ring bubble and then swim through it, apparently for amusement. D. McSweeny (private communication, 1990), a whale scientist, diver and professional photographer, has observed whales blowing ring bubbles. Vortex ring bubbles can be created by manually letting air bubbles into the neck of an inverted gallon jug filled with water.

There are several studies of vortex ring bubbles in the fluid dynamics literature. Turner (1957) has studied buoyant vortex rings, and includes constant-volume vortex ring bubbles as a special case. Turner used the concept of the impulse of a vortex ring to predict the spreading rate of the ring. Vortex ring bubbles were studied experimentally by Walters & Davidson (1963). These authors created vortex ring bubbles by rapidly opening and closing an air jet in the bottom of a water tank, obtaining ring bubbles with volumes from 6 to 110 cm^3. These are observed to spread as they rise as Turner predicted, but there were no measurements of the spreading rate. Pedley (1968) pointed out that vortex ring bubbles have a finite lifetime. Ultimately they are destroyed by surface tension instabilities. This will be discussed below.

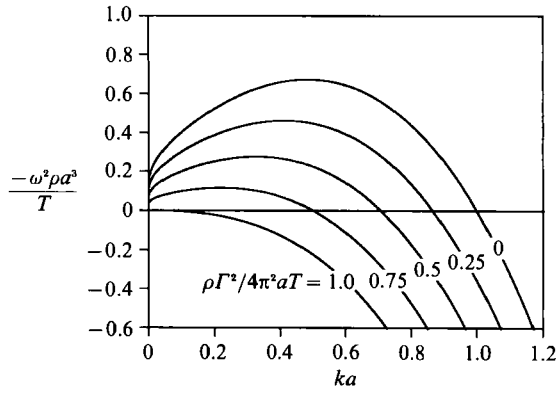

FIGURE 1. Growth rate versus wavenumber for a cylindrical bubble with circulation. Instability occurs when ω^2 is negative.

Large spherical cap bubbles can be created under conditions similar to those for vortex ring bubbles and are more frequently observed. Davies & Taylor (1950) created spherical cap bubbles, with volumes from 4.5 to 200 cm^3, by tilting an inverted beaker of air under water. It appears that large vortex ring bubbles and spherical cap bubbles of the same volume can be created by slightly different initial conditions.

The vortex ring bubbles described above are all of a fairly large size. Small vortex ring bubbles occur as a result of the collapse of cavitation bubbles near boundaries (Blake & Gibson 1987). The emphasis of the present study will be on large, persistent, gravitationally driven vortex ring bubbles.

Large vortex ring bubbles appear, from the observations cited above, to be very stable. Rayleigh (1892) showed that two-dimensional cylindrical bubbles are unstable to axially symmetric disturbances with wavelength longer than the circumference. Ponstein (1959) showed that circulation has a strongly stabilizing effect. Ponstein studied the stability of a two-dimensional bubble about which there is an irrotational swirling flow with $V_\theta = \Gamma_*/2\pi r$ for $r \geqslant a$, where a is the radius of a straight cylindrical bubble and Γ_* the circulation about it. For axially symmetric solutions of the form $\exp[\mathrm{i}(kz-\omega t)]$, the result is

$$\omega^2 = -\frac{kaK_1(ka)}{K_0(ka)}\left[(1-k^2a^2)\frac{T}{\rho a^3} - \frac{\Gamma_*^2}{4\pi^2a^4}\right], \tag{1.1}$$

where T is surface tension and ρ the density of the liquid. When $\Gamma_* = 0$ this is Rayleigh's result. Stability occurs when ω^2 is positive, therefore when

$$\frac{\Gamma_*^2}{4\pi^2a^4} \geqslant (1-k^2a^2)\frac{T}{\rho a^3}. \tag{1.2}$$

Stability occurs at all wavelengths when

$$\Gamma_*^2 \geqslant 4\pi^2 a\frac{T}{\rho}. \tag{1.3}$$

Stability curves are shown in figure 1. As Γ_* increases, the range of unstable wavenumbers shifts towards longer waves and the maximum growth rate becomes smaller until the flow becomes completely stable when (1.3) is satisfied. The steepness of the curves near $k = 0$ is caused by the logarithmic singularity of $K_0(ka)$.

Equation (1.3) would appear to show persistent stability for vortex ring bubbles, since the core radius a decreases slowly as the ring expands (assuming constant volume of the air core), thus strengthening the inequality. Pedley (1968) showed that viscous effects lead one to the opposite conclusion.

Pedley (1967) showed that if the swirling velocity outside a cylindrical bubble is not irrotational, but has circulation which increases outward from the bubble, the stability criterion for axially symmetric disturbances is the same as (1.2) and (1.3), with Γ_* in these expressions being the circulation about a contour *at the bubble surface*. That is, the stability depends only on the swirling velocity at the bubble surface and not on the surrounding vorticity distribution. In a later paper, Pedley (1968) applied this result to the stability of the viscous vortex ring bubble, modelling it as a cylindrical bubble in an axial strain field in order to allow for the decreasing radius of the bubble as the ring spreads. Zero shear stress at the bubble surface implies a continuous source of vorticity which diffuses outward, causing a slowly evolving rotational swirling flow. Since the circulation about a contour outside the rotational region must remain constant, the circulation around the bubble surface itself must decrease continually with time. He showed that the criterion (1.3) will finally be violated, despite the shrinking core radius, and the bubble will be destabilized. The bubble must rise a considerable distance before this occurs. Instability was not observed in Walters & Davidson's 3 ft high tank (Pedley estimated it would require a tank more than 5 ft deep), nor in the much greater distance (nearly 20 ft) exhibited in Earle & Giddings article. D. McSweeny (private communication, 1990) says vortex rings exhaled by divers can rise 50 to 60 ft before breaking up into a ring of smaller bubbles.

The purpose of this paper is to study the motion of vortex ring bubbles by means of a boundary-integral method. No other computations of vortex ring bubbles are known. The numerical aspects of the problem are very similar to those used by Lundgren & Mansour (1988); therefore, except for a brief review, only modifications required by the different geometry are presented. This material is to be found in §§3 and 4 and the results of the computations in §§5 and 6. Many aspects of our computations can be understood by means of a simple model equation which we present first in §2.

2. A model equation for a vortex ring bubble

The physics of vortex ring bubbles can be understood from a simple model equation which yields Turner's spreading law as a special case. We find some results which cannot be obtained by Turner's method.

The velocity of advance of a hollow circular vortex ring with circular section is given by the formula (Hicks 1884)

$$V_{\mathrm{B}} = \frac{\Gamma_*}{4\pi R}\left(\ln\frac{8R}{a} - \frac{1}{2}\right), \tag{2.1}$$

where R is the ring radius and a the core radius. This formula does not account for the buoyancy of the ring.

Let $\boldsymbol{u}$ be the velocity of a point on the ring centreline relative to the velocity given by (2.1). A force–momentum balance on a section of a slender ring, treated as locally two-dimensional, gives

$$\rho A\frac{\mathrm{d}\boldsymbol{u}}{\mathrm{d}t} = \rho\Gamma_*\,\hat{\boldsymbol{t}}\times\boldsymbol{u} + \rho A g\hat{\boldsymbol{k}}. \tag{2.2}$$

The term on the left is the apparent mass per unit length times acceleration. The bubble, being air filled, has little mass of its own. The apparent mass per unit length is the same as for a circular cylinder. The first term on the right is the Kutta–Joukowski lift per unit length on a vortex in a cross-flow. It acts perpendicularly to the relative velocity $\boldsymbol{u}$. The unit vector $\hat{\boldsymbol{t}}$ is along the centreline of the vortex, in the direction of the vorticity. The last term is the buoyancy force per unit length acting in an upward direction. We could add to this a surface tension force acting toward the centre of the ring. Equations of this kind, which use Kutta–Joukowski lift, have been discussed and used by Widnall & Bliss (1971), Moore & Saffman (1972) and Lundgren & Ashurst (1989).

Equation (2.2) is general enough that it could be applied to a non-circular vortex; however, we shall assume that it is circular with constant properties around the circumference. Then the cross-section area $A(=\pi a^2)$ is related to the ring radius R by a constant-volume assumption (which will be relaxed in future work)

$$2\pi RA = \tfrac{4}{3}\pi r_0^3, \tag{2.3}$$

where r_0 is the equivalent spherical radius of the bubble. Thus a in (2.1) can be given by

$$\frac{a}{r_0} = \left(\frac{2}{3\pi}\frac{r_0}{R}\right)^{\frac{1}{2}}. \tag{2.4}$$

The components of (2.2) yield the following system of dimensionless equations:

$$\frac{\mathrm{d}u}{\mathrm{d}t} = -\tfrac{3}{2}\Gamma R v, \tag{2.5}$$

$$\frac{\mathrm{d}v}{\mathrm{d}t} = \tfrac{3}{2}\Gamma R u + 1, \tag{2.6}$$

$$\frac{\mathrm{d}R}{\mathrm{d}t} = -u. \tag{2.7}$$

Here u is the horizontal velocity component, directed toward the centre of the ring for positive values, and v is the vertical component, positive upward. All lengths have been made dimensionless with r_0, all velocities have been made dimensionless with $(gr_0)^{\frac{1}{2}}$ and the time is made dimensionless with $(r_0/g)^{\frac{1}{2}}$. Effectively we have set $r_0 = 1$ and $g = 1$ in the equations. The circulation Γ which appears above is now the dimensionless quantity $\Gamma_*/(gr_0^3)^{\frac{1}{2}}$. We shall use these dimensionless variables in this section unless otherwise stated and again in §§5 and 6.

If the inertial terms are neglected (2.6) and (2.7) together have a simple solution:

$$u = -\frac{2}{3\Gamma R}, \tag{2.8}$$

$$R = R_{\mathrm{T}} = \left(R_0^2 + \frac{4t}{3\Gamma}\right)^{\frac{1}{2}}. \tag{2.9}$$

Equation (2.9) is Turner's result for a constant-volume buoyant vortex ring. Our interpretation is that the ring spreads radially at a velocity that gives just enough downward cross-flow lift to balance the upward buoyancy force. This is the direct physical reason for the radial growth of the ring.

We also note the possibility of oscillations, for if gravity is neglected in (2.6) and R is taken to be approximately constant there is a solution in which u and v are

sinusoidal with angular frequency $\omega = \frac{3}{2}\Gamma R$. This is exactly twice the (dimensionless) turnaround angular frequency of a fluid particle on the bubble surface. This means that the centre of the bubble core executes a circular trajectory with high frequency.

In general (2.5), (2.6) and (2.7) can be solved for large Γ by a multiple time expansion method described by Cole (1968). To get the equations into a convenient form we note that if we substitute u from (2.7) into (2.6) the equation can be integrated once. Then if u and v are eliminated by using (2.5) and (2.7) a single second-order differential equation for R results, namely

$$\frac{1}{\Gamma^2}\frac{\mathrm{d}^2R}{\mathrm{d}t^2} = \tfrac{3}{2}(t/\Gamma + \tfrac{3}{4}(R_0^2 - R^2)). \tag{2.10}$$

We have used the initial condition $v = 0$ at $t = 0$ and we shall also take $u = 0$ at that time. We introduce a slow time T and a fast time τ:

$$T = t/\Gamma, \tag{2.11}$$

$$\tau = \int_0^t \tfrac{3}{2}\Gamma R(t)\,\mathrm{d}t, \tag{2.12}$$

and assume that the solution is a function of both times so that

$$\frac{\mathrm{d}}{\mathrm{d}t} = \frac{1}{\Gamma}\frac{\partial}{\partial T} + \tfrac{3}{2}\Gamma R\frac{\partial}{\partial \tau}. \tag{2.13}$$

We then expand the solution in the form

$$R = R_{\mathrm{T}}(T) + \frac{1}{\Gamma^2}R_1(T,\tau) + \frac{1}{\Gamma^4}R_2(T,\tau) + \ldots \tag{2.14}$$

with Γ large. We find that R_1 must satisfy the partial differential equation

$$\frac{\partial^2 R_1}{\partial \tau^2} + R_1 = 0, \tag{2.15}$$

which has the solution

$$R_1(T,\tau) = A_1(T)\sin\tau + B_1(T)\cos\tau, \tag{2.16}$$

where the amplitudes A_1 and B_1 are unknown functions of the slow time. The equation for R_2 is the same as (2.16) but with a function of R_{T} and R_1 on the right-hand side. The amplitude functions are determined by requiring that secular terms be eliminated from the R_2 solution, i.e. by eliminating resonance driving terms from the right-hand side. The result is

$$A_1(T) = \frac{R_0^{\frac{1}{2}}}{R_{\mathrm{T}}^{\frac{1}{2}}}A_1(0) \tag{2.17}$$

$$B_1(T) = \frac{R_0^{\frac{1}{2}}}{R_{\mathrm{T}}^{\frac{1}{2}}}B_1(0) \tag{2.18}$$

The amplitudes decay slowly as the ring spreads. Since R_1 is zero at the initial time B_1 must be zero. However, in order to get the initial constant for A_1 we must calculate u. From (2.7) we find

$$u = -\frac{2}{3\Gamma R_{\mathrm{T}}} - \frac{3R_{\mathrm{T}}}{2\Gamma}A_1(T)\cos\tau + O(\Gamma^{-3}). \tag{2.19}$$

The first term on the right is the same as (2.8). The second, oscillating, term is of the same order as the first and cannot be neglected. The condition that u be zero at $t = 0$ gives

$$A_1(0) = -\left(\frac{2}{3R_0}\right)^2, \tag{2.20}$$

therefore using (2.16), (2.17) and (2.20) the final result for R is

$$R = R_T - \frac{1}{\Gamma^2}\frac{4}{9}\frac{\sin\tau}{R_T^{\frac{1}{2}}R_0^{\frac{3}{2}}} + O(\Gamma^{-4}) \tag{2.21}$$

with a small fast oscillation superimposed on Turner's solution. One should note that the oscillating part depends on the initial conditions and can be eliminated by a different choice. We cannot tell whether the natural starting condition for a vortex ring bubble will excite these oscillations. In any case it seems likely that oscillations could be excited by external disturbances.

The fast time can be calculated to lowest order by substituting R_T into (2.12). This gives

$$\tau = \tfrac{3}{4}\Gamma^2(R_T^3 - R_0^3). \tag{2.22}$$

A simple calculation shows that the frequency is approximately $\frac{3}{2}\Gamma R_T$, which varies slowly as the ring expands. This is double the instantaneous turnaround frequency. The slow increase in frequency is a consequence of a slow decrease in core radius while the circulation around the core remains constant.

Just as the buoyancy force causes radial growth of the vortex ring, surface tension will cause it to rise a little faster than (2.1). The surface tension force being directed toward the centre of the ring is balanced by an outward Kutta–Joukouwsky lift induced by positive v. Since persistent vortex ring bubbles are fairly large this is a small effect.

Viscous effects have been neglected in the above derivations. One might contemplate including a quasi-steady drag force per unit length in (2.2). However, as discussed by Pedley (1968), there can be no drag until the vorticity diffuses outward from the bubble surface and forms a wake. The bubble is likely to become unstable before this occurs.

The cross-flow lift term in (2.2) is essentially independent of the viscosity as long as the vorticity distribution is centred on the bubble core. In the force balance one merely considers the force on a cylinder large enough to enclose the vorticity. The inertial term would then be in error since one should include the mass between the bubble and the control cylinder as well as the apparent mass of this larger cylinder. We conclude that the integrity of (2.2) is maintained as long as the diffusing vortical layer is thin compared to the radius of the air core, i.e. $\nu t \ll a^2$. In dimensionless form this requires

$$t \ll a^2 \frac{(gr_0^3)^{\frac{1}{2}}}{\nu}. \tag{2.23}$$

The right-hand side is of order 1000 for typical large bubbles, large enough to allow many oscillation periods. Our computations in §6 only go to $t = 12$.

The nature of the oscillations discovered above may be understood from an exact two-dimensional potential flow solution which is given in some detail in the Appendix. This is generated from a well-known solution for a circular cylinder with circulation, executing any arbitrary motion, which consists of a two-dimensional

dipole oriented along the direction of the instantaneous velocity plus a line vortex. In the case under consideration the path of the centre of the cylinder is a circle of radius Δ, traversed at constant speed. One can calculate the pressure, and from this the force that one must apply to the cylinder in order to maintain this motion. It turns out by a simple calculation that if the angular frequency of the centre of the circle is twice the turnaround angular frequency the resultant force will vanish, i.e. the lift force will just balance the 'apparent' centrifugal force. This result is independent of Δ. In this self-balanced condition the local pressure on the surface is

$$\frac{p-p_\infty}{\rho} = \frac{1}{2}\left(\frac{\Gamma_*}{2\pi a}\right)^2\left(-12\frac{\Delta^2}{a^2}+32\frac{\Delta^2}{a^2}\cos^2\theta-1\right) \quad \text{(dimensional)}, \tag{2.24}$$

where θ is measured from the direction of the instantaneous velocity of the centre of the cylinder. The surface pressure is not constant, but has variations of only second order in Δ. This solution is therefore appropriate for small-amplitude oscillations of a cylindrical bubble. Surface tension would allow a solution in which the bubble shape differs slightly from circular, accommodating to the small pressure variation outside the bubble.

3. Boundary-integral method for bubbles

We consider the motion of gas-filled bubbles in an incompressible liquid. We adopt a description and numerical procedure used by Baker, Meiron & Orszag (1984) and Lundgren & Mansour (1988). Viscosity will be neglected and the liquid motion will be assumed to be irrotational. The gas in the bubble will be assumed to have uniform pressure. This is justified if the sound speed in the gas is large compared to the velocity scale in the liquid.

First we shall consider the case where the bubble volume is constant. It is filled with a fictititious incompressible fluid of negligible density compared to that of the surrounding fluid. The velocity potential ϕ is given by a distribution of dipoles over the bubble surface B, expressed by

$$\phi = \int_B \mu' \frac{\partial g(\boldsymbol{r}, \boldsymbol{r}')}{\partial n'} \mathrm{d}S, \tag{3.1}$$

where μ is the dipole density and

$$g(\boldsymbol{r}, \boldsymbol{r}') = -\frac{1}{4\pi|\boldsymbol{r}-\boldsymbol{r}'|} \tag{3.2}$$

is the velocity potential of a point source of unit strength. The normal here is taken *into* the bubble, outward from the liquid. The dipole representation ensures that the volume of the bubble stays constant.

The pressure in the liquid is determined from the Bernoulli equation,

$$\frac{\partial\phi}{\partial t}+\tfrac{1}{2}(\boldsymbol{u}\cdot\boldsymbol{u})+\frac{p}{\rho}+gz = \frac{p_\infty}{\rho}, \tag{3.3}$$

where p_∞ is the ambient pressure at the elevation $z = 0$. The boundary condition at the bubble surface requires that the pressure difference across the surface be balanced by surface tension forces,

$$p_1-p_b = T\,\mathrm{div}\,\hat{\boldsymbol{n}}, \tag{3.4}$$

where p_1 is the pressure on the liquid side of the interface, p_b is the bubble pressure, T is the surface tension and div $\hat{\boldsymbol{n}}$ is the curvature of the surface. Equations (3.3) and (3.4) together give an evolution equation for the velocity potential on the interface, namely

$$\frac{\mathrm{d}\phi_1}{\mathrm{d}t} - \tfrac{1}{2}(\boldsymbol{u}\cdot\boldsymbol{u}) + \frac{T}{\rho}\operatorname{div}\hat{\boldsymbol{n}} + gz = \frac{p_\infty - p_b}{\rho}, \tag{3.5}$$

where $\mathrm{d}/\mathrm{d}t$ is a material derivative.

The velocity on the interface is determined from the dipole density as follows. Upon taking the limit as the point $\boldsymbol{r}$ in (3.1) tends to the interface from the liquid side the Plemelj formula gives

$$\phi_1 = \tfrac{1}{2}\mu + \text{P.V.}\int_B \mu' \frac{\partial g(\boldsymbol{r},\boldsymbol{r}')}{\partial n'}\,\mathrm{d}S. \tag{3.6}$$

The tangential components of the velocity are determined from surface derivatives of ϕ_1. The normal component of the velocity is found from a vector potential $\boldsymbol{A}$, defined on the surface by

$$\boldsymbol{A} = -\text{P.V.}\int_B \mu'\hat{\boldsymbol{n}}' \times \nabla' g(\boldsymbol{r},\boldsymbol{r}')\,\mathrm{d}S', \tag{3.7}$$

using the formula

$$\boldsymbol{u}\cdot\hat{\boldsymbol{n}} = (\hat{\boldsymbol{n}}\times\nabla)\cdot\boldsymbol{A}, \tag{3.8}$$

which also only requires surface derivatives. Thus the velocity on the interface is given in terms of quantities defined on the interface. Points on the interface are evolved by

$$\frac{\mathrm{d}\boldsymbol{r}}{\mathrm{d}t} = \boldsymbol{u}. \tag{3.9}$$

The numerical procedure is therefore to use (3.5) and (3.9) to update the surface potential and the surface shape, then solve the integral equation (3.6) to obtain an updated value of μ from which the velocity can be computed for the next time step. However, there is an immediate problem because p_b is not known, so this procedure will not work without modification. There is a solvability condition which gets us out of this difficulty. This is where the analysis differs between drops and incompressible bubbles. Equation (3.6), regarded as an equation for μ when ϕ_1 is given, does not have a unique solution for bubbles. This may be seen from the exact integral

$$\text{P.V.}\int_B \frac{\partial g(\boldsymbol{r},\boldsymbol{r}')}{\partial n'}\,\mathrm{d}S = -\tfrac{1}{2}. \tag{3.10}$$

(Integrals of this kind may be evaluated by noting that the value is the volume flux across the surface from a unit source at the point $\boldsymbol{r}$. In (3.10) the point $\boldsymbol{r}$ is on the surface so half the flow goes away from the bubble and the other half goes through the surface in the negative direction.) This shows that the solution to (3.6) is only determined to within an arbitrary constant. Therefore the homogeneous adjoint equation

$$0 = \tfrac{1}{2}\tau + \text{P.V.}\int_B \tau' \frac{\partial g(\boldsymbol{r}',\boldsymbol{r})}{\partial n}\,\mathrm{d}S \tag{3.11}$$

has a non-trivial solution (but not simply a constant except for a spherical bubble). The condition that (3.6) be solvable is that ϕ_1 be orthogonal to τ, i.e.

$$\int_B \tau(\boldsymbol{r})\,\phi_1(\boldsymbol{r})\,\mathrm{d}S = 0. \tag{3.12}$$

In order to implement this we define a new variable

$$\tilde{\phi}_1 = \phi_1 + \int_0^t \frac{(p_\mathrm{b}-p_\infty)}{\rho}\,\mathrm{d}t, \tag{3.13}$$

so that (3.5) may be written

$$\frac{\mathrm{d}\tilde{\phi}_1}{\mathrm{d}t} - \tfrac{1}{2}(\boldsymbol{u}\cdot\boldsymbol{u}) + T/\rho\,\mathrm{div}\,\hat{\boldsymbol{n}} + gz = 0, \tag{3.14}$$

and then (3.6) becomes

$$\tilde{\phi}_1 - \int_0^t \frac{(p_\mathrm{b}-p_\infty)}{\rho}\,\mathrm{d}t = \tfrac{1}{2}\mu + \mathrm{P.V.}\int_B \mu' \frac{\partial g(\boldsymbol{r},\boldsymbol{r}')}{\partial n'}\,\mathrm{d}S. \tag{3.15}$$

This change of variables takes the pressure out of the differential equation and into the non-homogeneous part of the integral equation. We can now update $\tilde{\phi}_1$ with (3.14) and determine the pressure integral, and hence the bubble pressure, by the solvability condition

$$\int_0^t \frac{(p_\mathrm{b}-p_\infty)}{\rho}\,\mathrm{d}t = \frac{\int \tau\tilde{\phi}_1\,\mathrm{d}S}{\int \tau\,\mathrm{d}S}, \tag{3.16}$$

thus ensuring a unique solution.

This becomes more interesting, and more physical, if we allow for the compressibility of the bubble and approach the incompressible case in the limit. Compressibility may be accounted for by adding a time-dependent point source to the potential, so that the representation becomes

$$\phi = \int_B \mu' \frac{\partial g(\boldsymbol{r},\boldsymbol{r}')}{\partial n'}\,\mathrm{d}S + Q(t)\,g(\boldsymbol{r},\boldsymbol{r}_\mathrm{b}), \tag{3.17}$$

where $\boldsymbol{r}_\mathrm{b}(t)$ is a position inside the bubble. The tangential component of the velocity is calculated as before from surface derivatives of ϕ_1 (or $\tilde{\phi}_1$). The normal component is now obtained from

$$\boldsymbol{u}\cdot\hat{\boldsymbol{n}} = (\hat{\boldsymbol{n}}\times\nabla)\cdot\boldsymbol{A} + Q\frac{\partial g(\boldsymbol{r},\boldsymbol{r}_\mathrm{b})}{\partial n} \tag{3.18}$$

with $\boldsymbol{A}$ still defined by (3.7). The integral equation to determine μ becomes

$$\tilde{\phi}_1 - \int_0^t \frac{(p_\mathrm{b}-p_\infty)}{\rho}\,\mathrm{d}t - Q(t)\,g(\boldsymbol{r},\boldsymbol{r}_\mathrm{b}) = \tfrac{1}{2}\mu + \mathrm{P.V.}\int_B \mu' \frac{\partial g(\boldsymbol{r},\boldsymbol{r}')}{\partial n'}\,\mathrm{d}S, \tag{3.19}$$

and the solvability condition is now

$$\int_0^t \frac{(p_\mathrm{b}-p_\infty)}{\rho}\,\mathrm{d}t = \frac{\int \tau\tilde{\phi}_1\,\mathrm{d}S}{\int \tau\,\mathrm{d}S} - Q\frac{\int \tau g(\boldsymbol{r},\boldsymbol{r}_\mathrm{b})\,\mathrm{d}S}{\int \tau\,\mathrm{d}S}. \tag{3.20}$$

The bubble pressure is now related to the volume of the bubble and should be regarded as known, while the source strength $Q(t)$ is determined by this equation.

For an isentropic gas we can use

$$p_b = p_0(V/V_0)^{-\gamma}, \tag{3.21}$$

where

$$V_0 = \tfrac{4}{3}\pi r_0^3 \tag{3.22}$$

and

$$p_0 = p_\infty + \frac{2T}{r_0}. \tag{3.23}$$

Here we have defined V as the bubble volume, V_0 as a reference volume with equivalent spherical radius r_0, and p_0 is defined as the equilibrium pressure in a spherical bubble of radius r_0 at the ambient pressure p_∞. The bubble volume is related to the source strength by

$$\frac{dV}{dt} = Q \tag{3.24}$$

as may be seen from (3.18), since the vector potential part conserves volume.

We define a pressure-integral variable

$$I_p = \int_0^t \frac{(p_b - p_\infty)}{\rho}\, dt \tag{3.25}$$

so that

$$\frac{dI_p}{dt} = \frac{p_b - p_\infty}{\rho}. \tag{3.26}$$

The numerical strategy is to use (3.9), (3.14), (3.24) and (3.26) to update $\boldsymbol{r}$, $\tilde{\phi}_1$, V and I_p, solve (3.11) for τ in the updated geometry, determine an updated Q from (3.20), then solve (3.19) for updated μ. Then with μ and Q we can determine the updated velocity. Baker *et al.* (1984) have shown that both (3.11) and (3.19) may be solved by iteration.

The incompressible case may now be recovered from the compressible case by taking the incompressible limit $\gamma \to \infty$, which makes V constant ($V/V_0 = (p/p_0)^{-1/\gamma} \to 1$ as $\gamma \to \infty$) and hence makes Q zero (from (3.24)). Then (3.19) and (3.20) become the same as (3.15) and (3.16).

4. Modification for toroidal geometry

For a vortex ring bubble the circulation, Γ_*, around the ring cross-section must be specified. A dipole representation as in §3, with a continuous distribution of dipole density will give a single-valued velocity potential, hence no circulation. Restricting now to constant volume bubbles, we propose to represent the velocity potential in the form

$$\phi = \int_B \mu' \frac{\partial g(\boldsymbol{r}, \boldsymbol{r}')}{\partial n'}\, dS + \Phi_{\text{vor}}, \tag{4.1}$$

where Φ_{vor} is the velocity potential of a ring vortex of strength Γ_* with core coordinates $r_{\text{vor}}, z_{\text{vor}}$ which are inside the bubble cross-section. Φ_{vor} is given (Lamb 1932, §161) by a uniform dipole distribution of density Γ over the aperture disk. Φ_{vor} is discontinuous across the disk approaching $-\frac{1}{2}\Gamma_*$ from above and $\frac{1}{2}\Gamma_*$ from below. Thus the velocity potential consists of a continuous part represented by a smooth periodic dipole distribution over the bubble surface plus the discontinuous part Φ_{vor} which carries all the circulation. The velocity field generated is continuous and one can convince oneself that it is independent of the location of the ring core, a change

in core location being compensated by a modification in the continuous dipole distribution.

The velocity field is thus computed from two parts. One part from the concentrated vortex ring using the expressions for an axially symmetric vortex which can be deduced from Lamb (1932, §161); the second part from the smooth dipole distribution on the bubble surface, using the potential and vector potential method described in §3. In order to update the velocity potential on the bubble surface by (3.5) it is necessary to compute $\mathrm{d}\Phi_{\mathrm{vor}}/\mathrm{d}t$. This gives a numerical difficulty since Lagrangian nodal points can cross the disk discontinuity during a partial time step. To eliminate the need to deal with this we have performed this operation analytically by making use of the functional relationship

$$\Phi_{\mathrm{vor}} = F\left(\frac{z-z_{\mathrm{vor}}}{r_{\mathrm{vor}}}, \frac{r}{r_{\mathrm{vor}}}\right) \tag{4.2}$$

given by Lamb (1932, §161). Noting that the velocity generated by the concentrated vortex ring is

$$V_z = \frac{\partial \Phi_{\mathrm{vor}}}{\partial z}, \tag{4.3}$$

$$V_r = \frac{\partial \Phi_{\mathrm{vor}}}{\partial r} \tag{4.4}$$

we find, by the chain rule,

$$\frac{\mathrm{d}\Phi_{\mathrm{vor}}}{\mathrm{d}t} = V_z\left(u_z - \frac{\mathrm{d}z_{\mathrm{vor}}}{\mathrm{d}t} - \frac{z-z_{\mathrm{vor}}}{r_{\mathrm{vor}}}\frac{\mathrm{d}r_{\mathrm{vor}}}{\mathrm{d}t}\right) + V_r\left(u_r - \frac{r}{r_{\mathrm{vor}}}\frac{\mathrm{d}r_{\mathrm{vor}}}{\mathrm{d}t}\right), \tag{4.5}$$

where u_z and u_r are the velocity components at the point of interest. In order to compute this we need to specify how to compute z_{vor}, r_{vor} and their time derivatives. We have used the centroid of the bubble section for these coordinates. The centroid can be expressed as a line integral over the bubble interface and evaluated at each partial time step.

To implement this for an incompressible bubble we redefine $\tilde{\phi}_1$ (originally defined by (3.13)) as

$$\tilde{\phi} = \phi_1 + \int_0^t \frac{(p_{\mathrm{b}} - p_\infty)}{\rho}\,\mathrm{d}t - \Phi_{\mathrm{vor}}. \tag{4.6}$$

Then the integral equation becomes the same as (3.15) and the solvability condition the same as (3.16). Now $\tilde{\phi}_1$ is to be updated by

$$\frac{\mathrm{d}\tilde{\phi}_1}{\mathrm{d}t} + \frac{\mathrm{d}\Phi_{\mathrm{vor}}}{\mathrm{d}t} - \tfrac{1}{2}(\boldsymbol{u}\cdot\boldsymbol{u}) + \frac{T}{\rho}\operatorname{div}\hat{\boldsymbol{n}} + gz = 0. \tag{4.7}$$

One should notice that $\mathrm{d}\Phi_{\mathrm{vor}}/\mathrm{d}t$ is a continuous function of position. In the procedure described here it is not necessary to evaluate the discontinuous function Φ_{vor}.

5. Starting vortex ring bubbles

Walters & Davidson (1963) showed analytically that an initially spherical bubble will evolve toward a toroidal shape because of buoyancy forces. As the bubble begins to rise the vortex sheet which develops at the surface has a sense of rotation which induces motion of a tongue of liquid that pushes into the bubble from below. When

the bottom surface impinges on the upper surface the topology changes. We have simulated this initial-value problem numerically carrying the process further than Walters & Davidson could do analytically. This is done to assess the effect of surface tension which was neglected by them and to determine the circulation to use in the toroidal computations in §6. Unfortunately we can only compute until the two surfaces touch. The physics of the process beyond first contact is very complex, and appears to be similar to the impact of a raindrop on a free surface as described by Oguz & Prosperetti (1989). The impacting jet carries a thin air layer into the upper liquid which subsequently dissipates into small bubbles. During dissolution, the vorticity in the interfaces is transferred to circulation about a series of very thin annular vortex ring bubbles which in turn break up into strings of bubbles, presumably connected by thin viscous vortical regions in order to preserve circulation.

We have carried out these computations with 121 nodal points, time step 0.005 and different values of a dimensionless surface tension defined by

$$S = \frac{T}{\rho g r_0^2}. \tag{5.1}$$

In figure 2 (*a–e*) the results are shown for $S = 0.005, 0.025, 0.05, 0.1, 0.125$ which for water with $T = 75$ dyne/cm^3 correspond to bubbles with volumes 243.1, 22.8, 7.8, 2.7 and 1.9 cm^3, respectively. As the effect of surface tension increases the impinging jet becomes broader until in the last figure, where $S = 0.125$, it can no longer penetrate the upper interface and the separating layer of air thickens again so that the bubble becomes cup-shaped. For larger values of S the bubbles form shallower cups until at about $S = 1$ there is no indentation at the bottom at all and the bubble evolves into a disk-like shape. This suggests that small vortex ring bubbles cannot be created by this simple gravitational mechanism. In the cases where the jet penetrates and changes the topology we assume that the circulation about the resulting toroidal bubble is the difference in velocity potential between the bottom surface and the top surface at the point of contact. The dimensionless circulations for cases (*a*), (*b*), (*c*), (*d*) are computed to be 5.51, 5.16, 4.87 and 4.28, respectively, a rather narrow range of values compared to the range of bubble sizes.

The free evolution of an initially spherical bubble gives a mechanism for the creation of a toroidal bubble which is close to the experimental arrangement of Walters & Davidson and gives circulation values near those observed by them. It is difficult to see what is so different about the Davies & Taylor experiment that results in spherical cap bubbles. Spherical cap bubbles have turbulent parisitical trailing vortices and wakes. Somehow, because of differences in the external geometry and starting conditions, the flow must separate from the flanks of the evolving bubble before the penetrating jet can change the topology.

Computations similar to those shown above have been carried out by Baker & Moore (1989) for a two-dimensional bubble and compared with experiments of Walters & Davidson (1962). The main difference in the phenomena is that the penetrating jet becomes much broader and pinches off two side lobes from a symmetric cap, i.e. breaks into three pieces. Baker & Moore observed some numerical instabilities of a type that we did not observe in the present axially symmetric starting flows.

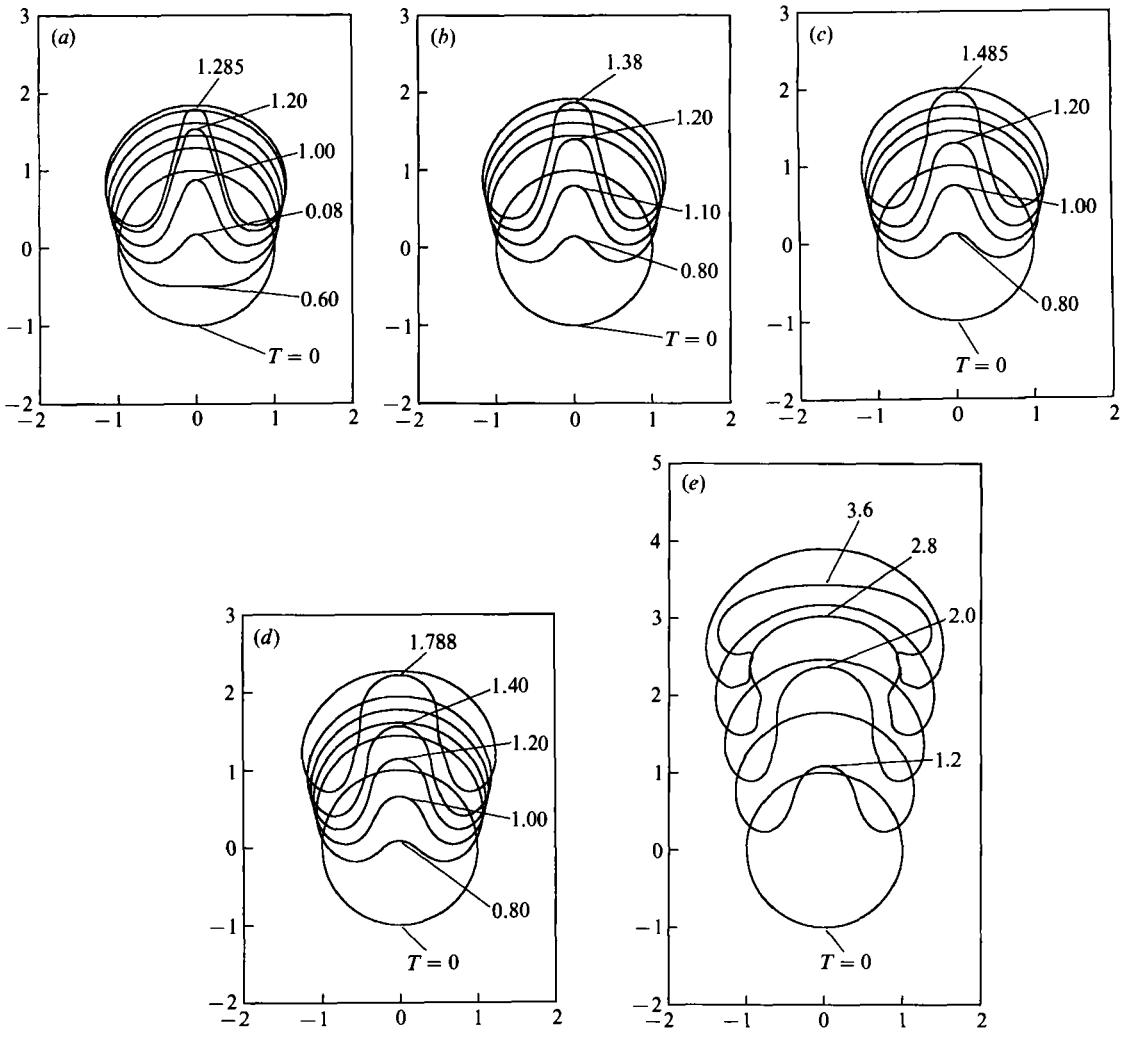

FIGURE 2. Evolution of an incompressible initially spherical bubble by buoyancy forces. (*a*) $S = 0.005$, final $\Gamma = 5.51$; (*b*) $S = 0.025$, final $\Gamma = 5.16$; (*c*) $S = 0.05$, final $\Gamma = 4.87$; (*d*) $S = 0.1$, final $\Gamma = 4.28$; (*e*) $S = 0.125$.

6. Computations of vortex ring bubbles

In this section we describe computations of the evolution of vortex ring bubbles by the method described in §4. We have used 61 nodal points and a time step of 0.005. The computations are started from a toroidal configuration with a circular core and several values of the radius ratio R/a. The initial value of $\tilde{\phi}_1$ (in (4.7)) is taken to be zero. Therefore the initial dipole distribution μ is zero, and the initial velocity induced by this dipole distribution is also zero. The initial velocity of the bubble surface is therefore determined from the concentrated vortex at the centre of the circular core. This is approximately the same as the hollow vortex velocity given by (2.1), but it is not quite constant over the circle (it would be constant if $R/a \to \infty$). The initial conditions are therefore not quite identical to those adopted for the model equation of §2.

For the first series we have taken $R/a = 5$ initially, a fairly large value in order to

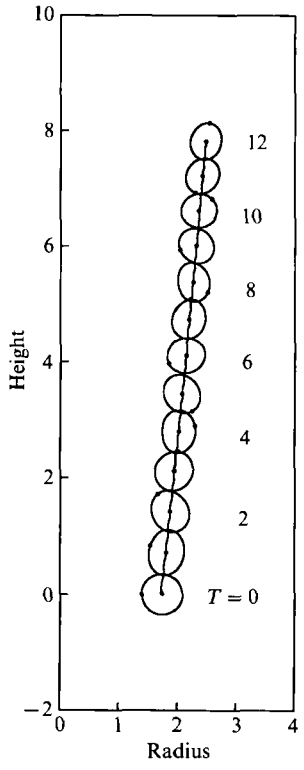

FIGURE 3. Cross-section shapes of an evolving vortex ring bubble. $S = 0.025$, initial $R/a = 5$, $\Gamma = 5$. The left-hand axis is the axis of symmetry of the ring.

minimize curvature effects, and we have taken $a = 0.3488$ to make the volume be $\frac{4}{3}\pi$, i.e. $r_0 = 1$. We have taken $\Gamma = 5$, which is in the range of possible values for the circulation. This value of Γ is large enough to satisfy the asymptotic requirements of the model equation solutions. We have taken $S = 0.025$ for the surface tension parameter, which corresponds to a volume of 22.8 cm^3 in water. (We have also repeated this series with $S = 0$ with only small differences.)

In figure 3 the successive shapes of the cross-section are plotted at dimensionless times 1 unit apart. The left coordinate axis is the symmetry axis of the vortex bubble. There are a number of things to be explained in this figure. First, it should be observed that the section shapes do not deviate very much from circular. Also the spreading rate is not large. Over the 12 time units of the computation the radius increases by only about 50%. The core area decreases noticeably as the radius increases. The black dots near the centres of the sections are at the centroids of the sections. We have included a curve on this figure which is the trajectory of the centroids. One can barely see oscillations on the trajectory. The black dots on the bubble surfaces are the positions of a marker which follows the fluid motion. From the bottom section to the next one up ($T = 1$) the marker has travelled once around the bubble in a clockwise sense, plus a little. The turnaround time is thus a little less than one time unit. If one computes it from $(2\pi a)^2/\Gamma$ one obtains 0.97 time units for the turnaround time. As the sections are followed through increasing times the marker gains a small amount at each circuit, until at the top of the figure the turnaround time is about $\frac{2}{3}$ of a unit, reflecting the reduction in core radius.

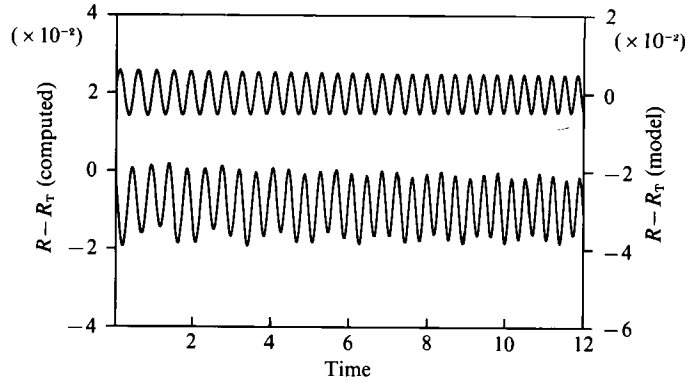

FIGURE 4. The difference between the radius of the vortex ring bubble and Turner's radius. $S = 0.025$, initial $R/a = 5$, $\Gamma = 5$. The upper curve and the right coordinate axis are for the model equation. The lower curve and the left coordinate axis are for the computations.

In order to compare the spreading of the ring radius with Turner's result we have plotted $R - R_T$ versus time, R being the computed radial coordinate of the centroid. This is the lower trace in figure 4 which uses the scale on the left axis. The upper trace is calculated from the model equation results (2.21) and (2.22). This curve uses the scale on the right axis. The only difference in the scales is the shift in the zero position. The period of the oscillations is observed to be about the same, the 1.5% difference is within the error of the asymptotics. However, the amplitudes of the oscillations differ by a factor of almost 2. We think this is because of the difference in the initial conditions described in the first paragraph of this section. There is also a small offset of the computed values from zero, the average value of R being less than R_T by about 0.01 unit. The overall agreement with the model is very good.

The pressure in the bubble results from a solvability condition as explained in §3. In figure 5(*a*) the pressure is plotted versus time in the lower curve. Pressure oscillations are clearly seen in this figure. The observed drop in pressure with time is mostly a consequence of the decrease in hydrostatic pressure as the bubble rises. However, the upper curve in figure 5(*a*), which is the pressure minus the hydrostatic pressure at the centroid, still shows an observable drop with time. This is caused by the variation in the dynamic pressure of the swirling part of the flow (which is the largest contribution to the velocity). The pressure on the surface of a two-dimensional bubble with circulation is smaller than the ambient pressure by $\frac{1}{2}\rho v_\theta^2$, or

$$\tfrac{1}{2}\rho\left(\frac{\Gamma_*}{2\pi a}\right)^2, \tag{6.1}$$

which increases in value as the core gets smaller. In figure 5(*b*) we have plotted the quantity

$$\frac{p}{\rho} + g z_{\text{cent}} + \frac{1}{2}\left(\frac{\Gamma_*}{2\pi a}\right)^2 \tag{6.2}$$

in dimensionless form at a larger scale. This accounts for most of the persistent variation of pressure with time. It remains to explain the very apparent pressure oscillations. They are not caused directly by the circular motion of the centre of the bubble section; according to (2.24) this would give a steady pressure. The oscillations of the radius of the ring causes the bubble area to pulsate (in order to conserve

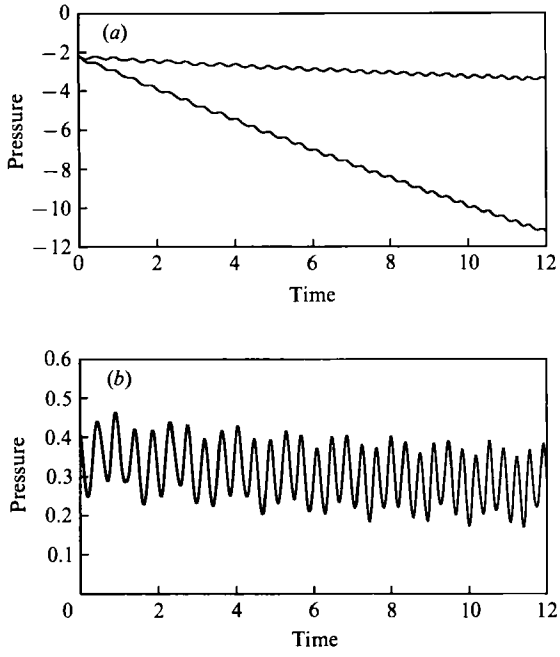

FIGURE 5. Pressure versus time. (*a*) The lower curve is the computed pressure, the upper curve is pressure minus hydrostatic pressure. (*b*) Pressure minus hydrostatic pressure plus the dynamic head of the swirling part of the flow.

volume) and we believe that this causes the pressure oscillations. In support of this assertion we note that the velocity potential of a ring source can be expressed in terms of elliptic integrals. Near the ring this potential is approximately

$$\phi = \frac{q}{2\pi} \ln \frac{8R}{r}, \tag{6.3}$$

where r is the distance from the bubble centroid. The source strength q is $\mathrm{d}A/\mathrm{d}t$, therefore the pressure at the surface of the bubble, which is related to the velocity potential by $p = -\rho \partial\phi/\partial t$ for small perturbations, is given by

$$\frac{p}{\rho} = -\frac{1}{2} \frac{\mathrm{d}^2 A}{\mathrm{d}t^2} \ln \frac{8R}{a}, \tag{6.4}$$

neglecting some smaller terms. Then determining A from (2.3) and using (2.21) we find the dimensionless result

$$p = -\frac{1}{3\pi} \frac{\ln (8R_{\mathrm{T}}/a)}{R_{\mathrm{T}}^{\frac{1}{2}} R_0^{\frac{3}{2}}} \sin \tau. \tag{6.5}$$

For the case under consideration where $R_{\mathrm{T}} \approx 5a$ and $a \approx 0.3488$ we find

$$p \approx -0.13 \sin \tau. \tag{6.6}$$

The amplitude 0.13 compares favourably with the amplitude of about 0.1 from figure 5(*b*) and the phase is right. This level of pressure fluctuation in a bubble of volume 22.8 cm^3 ($r_0 = 1.76$ cm) represents a sound level of 75 dB near the bubble, which should be detectable, and has a frequency of 50 Hz.

Figure 6 compares the computed axial velocity with Hicks' formula for the hollow vortex velocity V_{B} given by (2.1). It appears that V_{B} is an accurate average velocity.

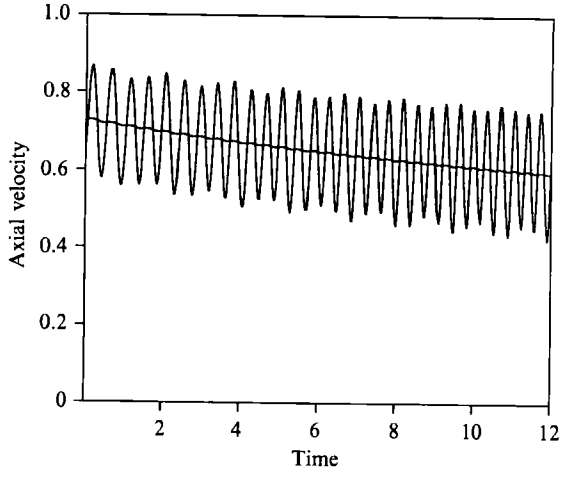

FIGURE 6. Axial velocity versus time. The oscillating curve is the computed axial velocity of the centroid. The smoother curve is Hicks' hollow vortex velocity.

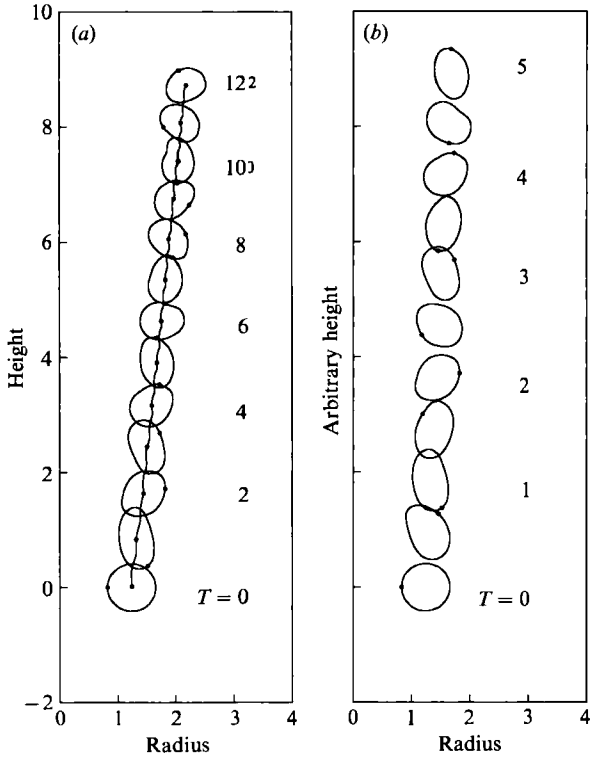

FIGURE 7. Cross-section shapes of an evolving vortex ring bubble. $S = 0.025$, initial $R/a = 3$, $\Gamma = 5$. (*a*) Compare with figure 3. (*b*) Intermediate shapes. Each section is displaced upward by one unit more than the section below it.

A second series with $R/a = 3$, $a = 0.413$, $\Gamma = 5$ and $S = 0.025$ is presented to show the effect of large curvature. In figure 7 (*a*) the section shapes are displayed. Now we see much larger deviations from circular because of the strain field of the smaller ring. However, from $T = 6$ onward the shapes look similar to the beginning of the $R/a = 5$

case. The early stages are shown with section shapes at intermediate times in figure 7(*b*). In this figure each section has been displaced upward by one more unit of length in order to prevent overlapping. What we are looking at here is the change of shape. Starting from a circular section the bubble becomes elongated at 1 and 1.5, more circular at 2 and 2.5, elongated again at 3 and 3.5 and so on. The behaviour is similar to that of a two-dimensional elliptical vortex, with uniform vorticity, in a plane-strain velocity field. An exact solution due to Kida (1981) shows that for small strain the ellipse rotates, stretching and slowing down when its major axis is oriented near a direction 45° past the direction of the principal axis with positive strain, and shortening and speeding up when it is perpendicular to this direction. In figure 7(*b*) the direction of positive strain, due to the finite vortex ring, is inclined 45° toward the axis of the ring, so that a line 45° past this direction is a vertical line. Indeed when the bubble is most elongated it is oriented near the vertical and the angular velocity of the bubble can be seen to be slower in this configuration. However, a full period of this rotation is about 4 turnaround times, which contrasts with a value near 2 turnaround times for the two-dimensional case with uniform vorticity.

The number of nodes used in this computation was 101 and the time step was 0.005. Results with 61 nodes were only slightly different but showed small surface oscillations of a type reported by Lundgren & Mansour (1988) and by others who have used boundary-integral methods.

7. Discussion and conclusions

Computations of the evolution of vortex ring bubbles were carried out using a modified boundary-integral method described in §§3 and 4. Because of the toroidal geometry, circulation about a loop through the bubble aperture must be specified for uniqueness. This problem was solved by representing the solution by a smooth dipole distribution over the bubble surface, plus a singular vortex ring located inside the bubble. The singular vortex ring carries the specified circulation. In a naturally occurring vortex ring bubble which evolves from a released spherical bubble, say, the circulation of the ring is determined by the starting process. We are unable to perform a single computation which follows the changing topology from sphere to toroid, therefore we have broken the process into two pieces. In the first computation a sphere evolves until the jet of fluid which penetrates the bubble from behind touches the upper part of the surface. Then we start a new computation starting from a toroidal geometry with the value of the circulation that developed from the first computation.

An added problem for all bubble geometries, not just toroidal, is non-uniqueness of the integral equation which determines the dipole density. In §3 it was shown how the required solvability condition determines the bubble pressure in the case of constant-volume bubbles.

The computations show that a vortex ring bubble grows as it rises, in agreement with Turner's (1957) predictions; however, the radius oscillates about Turner's result. These unexpected oscillations of the radius, and of the pressure, with a period one half of the turnaround time of a point on the bubble surface, were explained in §2 by means of a model equation, (2.2). The oscillations result from a self-balanced circular motion of the vortex core in which the centrifugal apparent mass force is balanced by the Kutta–Joukowski cross-flow lift.

Finally, we point out that the pressure oscillations may be large enough to be measurable by means of a hydrophone.

The authors would like to thank Dr K. Shariff for valued discussions. T.S.L. wishes to acknowledge support from the NASA Ames Research Center Director's Discretionary Fund and the Fluid Dynamics Division's Visiting Scientist Program, Contract NCA2-354, during the summer of 1989.

Appendix. Exact potential flow solution

The solution for the flow about a cylindrical body of radius a moving through an incompressible inviscid fluid which is at rest at infinity is given by the superposition of a two-dimensional dipole and a line vortex (Lamb 1932, §69). The velocity potential for this flow is

$$\phi(\boldsymbol{r},t) = -\frac{a^2\boldsymbol{U}\cdot(\boldsymbol{r}-\boldsymbol{R})}{|\boldsymbol{r}-\boldsymbol{R}|^2}+\frac{\Gamma\theta}{2\pi}, \quad \theta = \tan^{-1}\left(\frac{y-Y}{x-X}\right), \tag{A 1}$$

where $\boldsymbol{R}(t) = X(t)\hat{\boldsymbol{\imath}}+Y(t)\hat{\boldsymbol{\jmath}}$ is the instantaneous position of the centre of the cylinder and $\boldsymbol{U} = \boldsymbol{R}(t)$ is its velocity. The velocity field at a point in the flow is easily calculated to be

$$\boldsymbol{u}(\boldsymbol{r},t) = \nabla\phi = -\frac{a^2\boldsymbol{U}}{|\boldsymbol{r}-\boldsymbol{R}|^2}\cdot\left(I-2\frac{(\boldsymbol{r}-\boldsymbol{R})(\boldsymbol{r}-\boldsymbol{R})}{|\boldsymbol{r}-\boldsymbol{R}|^2}\right)-\frac{\Gamma}{2\pi}\frac{(\boldsymbol{r}-\boldsymbol{R})\times\hat{\boldsymbol{k}}}{|\boldsymbol{r}-\boldsymbol{R}|^2}, \tag{A 2}$$

where $\hat{\boldsymbol{k}}$ is a unit vector parallel to the axis of the cylinder. At a point, $\boldsymbol{r} = \boldsymbol{R}+a\hat{\boldsymbol{n}}$, on the cylinder, where $\hat{\boldsymbol{n}}$ is a unit radial vector, it is easily shown that the boundary condition $\boldsymbol{u}\cdot\hat{\boldsymbol{n}} = \boldsymbol{U}\cdot\hat{\boldsymbol{n}}$ is satisfied.

The pressure p in the flow may be found from the Bernoulli equation

$$\frac{p-p_\infty}{\rho} = -\frac{\partial\phi}{\partial t}-\tfrac{1}{2}(\boldsymbol{u}\cdot\boldsymbol{u}) \tag{A 3}$$

with $\partial\phi/\partial t$ calculated from (A 1) as

$$\frac{\partial\phi}{\partial t} = -\frac{a^2\dot{\boldsymbol{U}}\cdot(\boldsymbol{r}-\boldsymbol{R})}{|\boldsymbol{r}-\boldsymbol{R}|^2}-\boldsymbol{U}\cdot\boldsymbol{u}. \tag{A 4}$$

In particular the pressure on the surface of the cylinder is given by

$$\frac{p-p_\infty}{\rho} = -\tfrac{3}{2}\boldsymbol{U}\cdot\boldsymbol{U}+2(\boldsymbol{U}\cdot\hat{\boldsymbol{n}})^2-\frac{1}{2}\left(\frac{\Gamma}{2\pi a}\right)^2-\frac{\Gamma}{\pi a}\hat{\boldsymbol{n}}\times\hat{\boldsymbol{k}}\cdot\boldsymbol{U}+a\ddot{\boldsymbol{R}}\cdot\hat{\boldsymbol{n}}. \tag{A 5}$$

The external force $\boldsymbol{F}$ which is required to produce this arbitrary motion is given by

$$\boldsymbol{F} = \int_0^{2\pi}(p-p_\infty)\,\hat{\boldsymbol{n}}a\,\mathrm{d}\theta = \rho\pi a^2\ddot{\boldsymbol{R}}-\rho\Gamma\hat{\boldsymbol{k}}\times\boldsymbol{U}. \tag{A 6}$$

Therefore, if the cylinder is massless (a bubble) and has no applied forces, its motion must be governed by

$$\rho\pi a^2\ddot{\boldsymbol{R}} = \rho\Gamma\hat{\boldsymbol{k}}\times\dot{\boldsymbol{R}}, \tag{A 7}$$

that is, the apparent mass times acceleration must be balanced by the Kutta–Joukowski lift, i.e. acceleration perpendicular to velocity. The only possible motion is constant speed along a circular path;

$$\boldsymbol{R} = \Delta(\hat{\boldsymbol{\imath}}\cos\omega t+\hat{\boldsymbol{\jmath}}\sin\omega t) \tag{A 8}$$

satisfies the equation with constant circular radius Δ and angular frequency

$$\omega = \frac{\Gamma}{\pi a^2} \tag{A 9}$$

which is independent of the radius of the circle.

REFERENCES

Baker, G. R., Meiron, D. I. & Orszag, S. A. 1984 Boundary integral methods for axisymmetric and three-dimensional Rayleigh–Taylor instability problems. *Physica* **12D**, 19–31.

Baker, G. R. & Moore, D. W. 1989 The rise and distortion of a two-dimensional gas bubble in an inviscid liquid. *Phys. Fluids* A **1**, 1451–1459.

Blake, J. R. & Gibson, D. C. 1987 Cavitation bubbles near boundaries. *Ann. Rev. Fluid Mech.* **19**, 99–123.

Cole, J. D. 1968 *Perturbation Methods in Applied Mathematics.* Blaisdell.

Davies, R. M. & Taylor, G. I. 1950 The mechanics of large bubbles rising through extended liquids and through liquids in tubes. *Proc. R. Soc. Lond.* A **200**, 375–390.

Earle, S. A. & Giddings, A. 1976 Life springs from death in Truk lagoon. *Natl Geog. Mag.* **149**, 578–603.

Hicks, W. M. 1884 On the steady motion and small vibrations of a hollow vortex. *Phil. Trans. R. Soc. Lond.* A **175**, 183.

Kida, S. 1981 Motion of an elliptic vortex in a uniform shear flow. *J. Phys. Soc. Japan* **50**, 3517–3520.

Lamb, H. 1932 *Hydrodynamics.* Cambridge University Press.

Lundgren, T. S. & Ashurst, W. T. 1989 Area-varying waves on curved vortex tubes with application to vortex breakdown. *J. Fluid Mech.* **200**, 283–307.

Lundgren, T. S. & Mansour, N. N. 1988 Oscillations of drops in zero gravity with weak viscous effects. *J. Fluid Mech.* **194**, 479–510.

Moore, D. W. & Saffman, P. G. 1972 The motion of a vortex filament with axial flow. *Phil. Trans. R. Soc. Lond.* A **272**, 407–429.

Oguz, H. N. & Prosperetti, A. 1989 Surface-tension effects in the contact of liquid surfaces. *J. Fluid Mech.* **203**, 149–171.

Pedley, T. J. 1967 The stability of rotating flows with a cylindrical free surface. *J. Fluid Mech.* **30**, 127–147.

Pedley, T. J. 1968 The toroidal bubble. *J. Fluid Mech.* **32**, 97–112.

Ponstein, J. 1959 Instability of rotating cylindrical jets. *Appl. Sci. Res.* A **8**, 425–456.

Rayleigh, Lord 1892 On the instability of cylindrical fluid surfaces. *Phil. Mag.* **34**, 177–80.

Turner, J. S. 1957 Buoyant vortex rings. *Proc. R. Soc. Lond* A **239**, 61–75.

Walters, J. K. & Davidson, J. F. 1962 The initial motion of a gas bubble formed in an inviscid liquid. Part 1. The two-dimensional bubble. *J. Fluid Mech.* **12**, 408–416.

Walters, J. K. & Davidson, J. F. 1963 The initial motion of a gas bubble formed in an inviscid liquid. Part 2. The three-dimensional bubble and the toroidal bubble. *J. Fluid Mech.* **17**, 321–336.

Widnall, S. & Bliss, D. 1971 Slender-body analysis of the motion and stability of a vortex filament containing an axial flow. *J. Fluid Mech.* **50**, 335–353.